HHS Public Access

Author manuscript

J Pathol. Author manuscript; available in PMC 2023 October 20.

Published in final edited form as:

J Pathol. 2020 July ; 251(3): 323–335. doi:10.1002/path.5456.

Effect of VEGFC on lymph flow and inflammation-induced alveolar bone loss

Hua Wang[1,2,†], **Yuyi Chen**[1,2,†], **Wenlei Li**[1,2,†], **Lian Sun**[1,2], **Hongyu Chen**[1,2], **Qiudong Yang**[1,2], **Hang Zhang**[1,2], **Weibing Zhang**[1,2], **Hua Yuan**[1,2], **Hengwei Zhang**[3], **Lianping Xing**[3], **Wen Sun**[1,2,*]

[1]Jiangsu Key Laboratory of Oral Diseases, Nanjing Medical University, Nanjing, PR China

[2]Department of Basic Science of Stomatology, Affiliated Hospital of Stomatology, Nanjing Medical University, Nanjing, PR China

[3]Department of Pathology and Laboratory Medicine and Center for Musculoskeletal Research, University of Rochester Medical Center, Rochester, New York, USA

Abstract

The lymphatic system plays a crucial role in the maintenance of tissue fluid homeostasis and the immunological response to inflammation. The effects of lymphatic drainage dysfunction on periodontitis have not been well studied. Here we show that lymphatic vessel endothelial receptor 1 $(LYVE1)^+$/podoplanin $(PDPN)^+$ lymphatic vessels (LVs) are increased in the periodontal tissues, with accumulation close to the alveolar bone surface, in two murine periodontitis models: rheumatoid arthritis (RA)-associated periodontitis and ligature-induced periodontitis. Further, $PDPN^+$/alpha-smooth muscle actin $(\alpha SMA)^-$ lymphatic capillaries are increased, whereas $PDPN^+/\alpha SMA^+$ collecting LVs are decreased significantly in the inflamed periodontal tissues. Both mouse models of periodontitis have delayed lymph flow in periodontal tissues, increased TRAP-positive osteoclasts, and significant alveolar bone loss. Importantly, the local administration of adeno-associated virus for vascular endothelial growth factor C, the major growth factor that promotes lymphangiogenesis, increases the area and number of $PDPN^+/\alpha SMA^+$ collecting LVs, promotes local lymphatic drainage, and reduces alveolar bone loss in both models of periodontitis. Lastly, $LYVE1^+/\alpha SMA^-$ lymphatic capillaries are increased, whereas $LYVE1^+/\alpha SMA^+$ collecting LVs are decreased significantly in gingival tissues of patients with chronic periodontitis compared with those of clinically healthy controls. Thus, our findings reveal an important role of local lymphatic drainage in periodontal inflammation-mediated alveolar bone loss.

*Correspondence to: W Sun, Jiangsu Key Laboratory of Oral Diseases, Nanjing Medical University, 140 Hanzhong Road, Nanjing 210029, PR China. wensun@njmu.edu.cn.

†These authors contributed equally to this work.

Author contributions statement

HW, YC, WL, LS, HC, QY, HZ, WZ, HY, HZ, LX, and WS contributed to study design. HW, YC, WL, HZ, and WS contributed to study conduct. HW, YC, WL, and WS collected data. HW, LS, HC, QY, and WS analyzed data. HW, YC, WL, WZ, HY, HZ, LX, and WS interpreted data. HW, YC, WL, and WS drafted the manuscript. HZ, LX, and WS revised manuscript content. HW, YC, WL, LS, HC, QY, HZ, WZ, HY, HZ, LX, and WS approved the final version of the manuscript. WS takes responsibility for the integrity of the data analysis.

Reference 58 is cited only in the supplementary material.

Keywords

alveolar bone loss; lymphatic drainage; periodontitis; TNF-Tg mice; VEGFC

Introduction

The lymphatic system plays a major role in the maintenance of tissue fluid homeostasis and the immunological response to inflammation [1–3]. The lymphatic system consists of all lymphatic vessels (LVs) and lymphoid organs. In the peripheral tissues, lymphatic capillaries, which are initial LVs and composed of single-layer lymphatic endothelial cells (LECs), allow soluble cellular wastes, immune cells, and particulate matter to enter the lymphatic system [4–6]. The collected fluid and cells form lymph, which is then transported by collecting LVs that are composed of LECs and smooth muscle cells (SMCs) to the draining lymph nodes [4,7]. The lymph node, mainly containing B cells and T cells, provides a highly organized microarchitecture that supports optimal immune defense [8]. Lymphatic capillaries, collecting LVs, and lymph nodes together provide the defensive line against infection for the body.

Periodontitis is a common chronic inflammatory disease characterized by osteoclast-mediated bone resorption and periodontal attachment loss. Recently, more attention has been paid to the association between oral health and chronic autoimmune inflammatory diseases [9–11]. Rheumatoid arthritis (RA) is a chronic, destructive autoimmune inflammatory disorder which causes bone erosion and joint deformity [12,13]. A number of clinical and epidemiologic studies have suggested associations between RA and periodontitis [10,11]. Peri10,11]. Periodontal inflammation and alveolar bone loss have been reported in the genetically modified TNF-transgenic (Tg) RA mouse model [14]. Another widely-used mouse model for a periodontitis study is ligature-induced periodontitis, in which the disease can be triggered at a designated time, with periodontal inflammation and alveolar bone loss occurring within a few days [15].

As peripheral tissue, the periodontal tissue also contains LVs [16–21], which drain to the cervical lymph nodes in mice [16,20,22]. A previous study has reported that LVs present in the periodontal tissue partly protect against periodontitis [16]. This study clearly demonstrated that mice carrying the K14-vascular endothelial growth factor (VEGF) receptor 3 (VEGFR3)-Ig transgene lack LVs in gingiva. They have more periodontal bone resorptive activity, stronger inflammatory immune responses, and also weaker humoral immune responses after *Porphyromonas gingivalis* challenge than their wild-type (WT) littermates [16]. Vascular endothelial growth factor C (VEGFC) is the major growth factor that promotes lymphangiogenesis, and it exerts most of its effects through binding to VEGFR3 [23]. However, a transgenic mouse model of VEGFC overexpression, under the control of the K14 promoter, showed that hyperplastic lymphatics do not protect against the development of ligature-induced periodontitis [20]. It is possible that the K14 promoter only directs target gene expression in epithelium [24]. It is reported that relatively thick LVs, distributed sparsely and located apart from the epithelia, appeared to pass through the lamina propria of the gingiva toward the alveolar crest, and run along the external surface of the

alveolar bone [25]. We speculate that these relatively thick LVs may exert major effects on lymphatic drainage and further on periodontal inflammation-mediated alveolar bone loss.

In this study, we hypothesized that lymphatic dysfunction is associated with alveolar bone loss, while VEGFC overexpression might promote local lymphatic drainage and reduce alveolar bone loss in periodontal tissues of periodontitis. We used two mouse models of periodontitis (RA-associated periodontitis, by using TNF-Tg mice, and ligature-induced periodontitis) and tissues of patients with chronic periodontitis, and demonstrated an important role of local lymphatic drainage in periodontal inflammation-mediated alveolar bone loss.

Materials and methods

Animals

We used two mouse models of periodontitis: (1) RA-associated periodontitis and (2) ligature-induced periodontitis. For RA-associated periodontitis, TNF-transgenic (Tg) mice (the TNF-Tg line 3647) were kindly provided by Dr G Kollias and had been crossed with C57BL/6J mice for more than ten generations [26]. This line of TNF-Tg mice carries a modified human *TNF* transgene in which the 3′-region of the *TNF* gene is replaced with that of the human α-globin gene [27]. We have demonstrated that arthritis develops in the ankles of these mice at ~2 months of age and progresses, leading to systemic bone loss and osteoporosis at ~4 months of age [28]. We used male TNF-Tg mice for all *in vivo* experiments because female TNF-Tg mice develop joint lesions earlier and die around 6 months old due to lung inflammation [29]. For the second model, ligature-induced periodontitis, experimental periodontitis was induced in 2-month-old WT male mice as described, with modifications [30]. In brief, a 5–0 silk ligature was placed in the submarginal position on the left maxillary first molar and the contralateral tooth was left unligated to serve as the baseline control. The mice were sacrificed and analyzed 14 days after placement of the ligature. All mice were bred and maintained in the SPF Laboratory Animal Center of Nanjing Medical University. The use of animals in this study was approved by the Institutional Animal Care and Use Committee of Nanjing Medical University (Approval ID1906018).

Patients and sampling

Detailed written informed consent was obtained from all volunteers in accordance with protocols approved by the Human Subjects Institutional Review Board of Nanjing Medical University (Approval ID 2016115). Gingival tissues were obtained from subjects with clinically healthy gingiva and patients with severe chronic periodontitis as previously reported [31]. Apart from the chronic periodontitis, all subjects were in good general health and had not taken anti-bacterial or anti-inflammatory drugs within the 3 months before sampling. Subjects with clinically healthy gingiva showed no bleeding on probing, probing depth < 3 mm, and no attachment loss or alveolar bone loss. Healthy gingival tissue specimens were collected during tooth extraction for orthodontic reasons. Subjects with severe chronic periodontitis showed bleeding on probing, probing pocket depth > 6 mm, and alveolar bone loss greater than 60% of the root. Gingival tissues from patients with severe

chronic periodontitis were collected from teeth extracted after determining that the tooth was untreatable. The collected specimens were immediately placed in a sterile tube containing αMEM medium (Gibco, Grand Island, NY, USA) and transferred to the laboratory for study within 2 h, mainly for histology, immunofluorescence staining, single cell preparation, and flow cytometry.

Radiological study

Maxillae were removed and dissected free of all soft tissues for micro-computed tomography (micro-CT; Scanco Medical, Bassersdorf, Zurich, Switzerland) as described previously [32].

Histology and histochemical staining

Details are provided in supplementary material, Supplementary materials and methods.

Immunofluorescence staining

Isolated maxillae, cervical lymph nodes of murine samples or gingival tissues of human specimens were fixed in 10% neutral buffered formalin and then the maxillae were decalcified in 10% EDTA. All samples, including the decalcified murine maxillae, were dehydrated and embedded in paraffin wax and 4-μm sections were cut using a rotary microtome (Leica, Wetzlar, Germany). The deparaffinized sections were subjected to antigen retrieval, blocked in PBS with 10% normal goat serum and 0.2%TritonX-100for 1 h, and then stained overnight with rabbit anti-LYVE1 (cat # ab14917, 1:200; Abcam, Cambridge, UK) or hamster anti-PDPN (cat # ab11936, 1:200; Abcam) or FITC-labeled anti-αSMA (cat # F3777, 1:500; Sigma-Aldrich, St Louis, MO, USA) or rat anti-B220 (cat # 553086, 1:50; BD Pharmingen, San Diego, CA, USA) or rabbit anti-CD3 (cat # 99940, 1:100; Cell Signaling Technology, Danvers, MA, USA) or rat anti-F4/80 (cat # ab16911, 1:50 Abcam) at 4 °C. After rinsing with PBS for 15 min, tissues were incubated with goat anti-rabbit Alexa Fluor 488, or goat anti-hamster Alexa Fluor 568, goat anti-rat Alexa Fluor 488, or goat anti-rabbit Alexa Fluor 568 (1:400; Invitrogen, Carlsbad, CA, USA) at room temperature. Slides were mounted with Mounting Medium containing DAPI (Vector Labs, Burlingame, CA, USA) and images were captured using a Leica DM4000 fluorescence microscope, as reported previously [33].

In vivo lymph flow measurements

Indocyanine green (ICG)-near infrared (NIR) lymphatic imaging was performed by injecting ICG (Sigma-Aldrich) sub-epithelially into buccal oral mucosa, and the dynamics of ICG fluorescence was visualized under infrared laser illumination and recorded, as previously described, with modifications [20]. In brief, 1 μl (0.5 μg/μl) of ICG was injected sub-epithelially in the buccal oral mucosa to the maxillary first molar area using a graded Hamilton syringe (34-G needle). The total fluorescence in the entire posterior facial area was measured in an optical imager by IVIS Spectrum (PerkinElmer, Waltham, MA, USA) at 60 min post-injection. The measurement was repeated every 90 min for a 7-h period. The mice were awake and able to move freely between measurements. Lymphatic drainage, as indicated by the percentage of ICG clearance, was assessed by calculating the percentage

difference of ICG signal intensity between the detected time points and 60-min NIR scans from the regions of interest after ICG injection [34].

Administration of AAV-VEGFC vector

A recombinant adeno-associated virus (AAV) encoding a full-length human VEGFC cDNA (NM_005429) was purchased from Genechem Biotech Inc (Shanghai, PR China). We have used the same human VEGFC cDNA to generate AAV-VEGFC and have demonstrated the expression of a 29 kDa secreted form of human VEGFC by western blotting analysis of the conditioned media collected from AAV-VEGFC-infected cells previously [35]. The recombinant AAV virions were purified by the supplying company. Transduction consisted of injecting the viral vectors in a site-specific manner as previously described, with modifications [36]. In brief, 1 μl of viral solution (10^{10} viral particles per μl) was injected sub-epithelially in the buccal oral mucosa to the maxillary first molar area using a graded Hamilton syringe (34-G needle) at the time specified in the figure legends. AAV transduction efficiency was determined by RT-qPCR as described in supplementary material, Supplementary materials and methods.

Flow cytometry

Cells were harvested from cervical lymph nodes, periodontal tissues of murine samples or gingival tissues of human specimens and analyzed by flow cytometry using the antibodies and methods presented in supplementary material, Supplementary materials and methods.

Statistical analysis

All results are given as mean ± SD or as specified in the figure legends. Statistical analysis was performed using GraphPad Prism 5 software (GraphPad Software Inc, San Diego, CA, USA). Comparisons between two groups were analyzed using the two-tailed unpaired Student's *t*-test. Comparisons among three or more groups were carried out using one-way ANOVA followed by Dunnett's *post hoc* multiple comparisons test. *P* values less than 0.05 were considered statistically significant.

Results

Increased alveolar bone loss, TRAP-positive osteoclasts, and lymphatic vessel areas in RA-associated periodontitis

Periodontitis-like phenotypes have been reported in TNF-transgenic (Tg) mice [14]. To examine RA-mediated periodontal bone loss in TNF-Tg mice, micro-CT (μCT) and morphometric analyses were performed on the mouse maxillae. Three-dimensional reconstruction images and volumetric measurements from μCT analysis revealed alveolar bone loss and a significantly higher level of exposed root surface in the maxillae of TNF-Tg mice compared with WT mice (Figure 1A,B). Furthermore, morphometric measurements of H&E-stained tissue sections showed that the distance from the cemento-enamel junction (CEJ) to the alveolar bone crest (ABC) was significantly greater in TNF-Tg mice than in WT mice (Figure 1C,D). Osteoclastic bone resorption in dental alveolar bone was also examined in paraffin-embedded sections stained histochemically for TRAP. TRAP-positive osteoclast surface was markedly larger in TNF-Tg mice than in WT mice (Figure 1E,F).

At the tissue level, LVs can be identified by immunostaining with antibodies to lymphatic vessel endothelial receptor 1 (LYVE1) [37,38] or podoplanin (PDPN) [39,40], proteins specifically expressed by LECs. To study the distribution of LVs in periodontal tissue, paraffin-embedded tissue sections from TNF-Tg and WT mice were double-stained with anti-LYVE1 and anti-PDPN antibodies. We observed numerous $LYVE1^+/PDPN^+$ LVs in the periodontal soft tissues around the alveolar bone crest (Figure 1G,H). Interestingly, $PDPN^+$ LVs were occasionally negative for LYVE1; however, no certain relationship was identified (Figure 1G). More importantly, the $LYVE1^+/PDPN^+$ area (%) in periodontal tissue was significantly greater in TNF-Tg mice than in WT mice (Figure 1G,H). In addition, we performed subsequent experiments using mesial periodontal tissues of the maxillary first molar because the distribution of LVs was close to areas of bone destruction (Figure 1G).

Numbers of lymphatic endothelial cells, macrophages, and B cells are increased in periodontal tissues and in the cervical (draining) lymph nodes in RA-associated periodontitis

The lymphatic system plays a crucial role in balancing tissue fluid and organizing the immunologic response to inflammation by removing extra fluid and enabling trafficking of immune cells to the draining lymph nodes [20]. We next searched potential effects of the increased LVs in RA-associated periodontitis by examining cell populations via flow cytometry. The data suggested that the percentages of $CD31^+PDPN^+$ LECs, $CD45.2^+F4/80^+$ macrophages, and $B220^+$ B cells were all markedly higher in periodontal tissues from TNF-Tg mice than in those from WT mice (Figure 2A,B).

To further study the immune cell composition in the cervical (draining) lymph nodes, we used flow cytometry with markers for various cell types. The data revealed that the percentages of $PDPN^+$ LECs, $CD45.2^+F4/80^+$ macrophages, and $B220^+$ B cells were all evidently greater in cervical lymph nodes from TNF-Tg mice than in those from WT mice (Figure 2C,D). In contrast, the percentage of $CD3^+$ T cells was significantly lower in TNF-Tg mice than in WT mice (Figure 2C,D). Additionally, IF staining confirmed that there was an increased number of $LYVE1^+/PDPN^+$ LECs, associated with which there were numerous $B220^+$ B cells and $F4/80^+$ macrophages infiltrating into the cervical lymph nodes from TNF-Tg mice compared with those from WT mice (Figure 2E,F). Besides, the lymph node expansion is notable as determined by H&E staining (Figure 2E), which is typical for the TNF-Tg model [41,42].

Decreased collecting lymphatic vessels and lymph flow in periodontal tissues of RA-associated periodontitis

Given the markedly increased LVs with infiltration of numerous immune cells in periodontal tissues of TNF-Tg mice, we next examined the function of these LVs. In addition to valves, collecting LVs are distinguished from capillary lymphatics by the presence of both LECs and SMCs [7], which contract to pump lymph. Since SMCs express alpha-smooth muscle actin (αSMA), double immunofluorescence staining with anti-PDPN and anti-αSMA antibodies is used in most studies to identify collecting LVs [7,43]. Using IF, we observed three types of vessels: $PDPN^+/\alpha SMA^-$ lymphatic capillaries, $PDPN^+/\alpha SMA^+$ collecting LVs, and $PDPN^-/\alpha SMA^+$ blood vessels in periodontal tissues of WT mice (Figure 3A).

Notably, more $PDPN^+/\alpha SMA^-$ lymphatic capillaries could be seen in periodontal tissues of TNF-Tg mice than in those of WT mice (Figure 3A,B). In contrast, few $PDPN^+/\alpha SMA^+$ collecting LVs were observed in periodontal tissues of TNF-Tg mice compared with those of WT mice (Figure 3A,B).

To further assess function of the increased LVs, periodontal lymphatic drainage indicated by the percentage of ICG clearance was assessed by calculating the percentage difference of ICG signal intensity between the detected time points and 60-min NIR scans from the regions of interest after ICG injection. Compared with the periodontal areas of WT mice, periodontal areas of TNF-Tg mice had markedly delayed ICG clearance (Figure 3C). At time points 330 and 420 min, the percentage of ICG clearance was significantly lower in periodontal tissues of TNF-Tg mice than in those of WT mice, respectively (Figure 3C).

To explore the mechanisms responsible for increased LVs in TNF-Tg mice, we examined the expression of genes using gingival tissues by RT-qPCR. The expression of genes, including *Vegfc*, *Vegfd*, and the ratio of *Vegfc* to *Vegfd* mRNA levels, was significantly upregulated in TNF-Tg mice compared with their WT littermates. In contrast, the expression of *Vegfr3* was downregulated clearly in gingival tissues of TNF-Tg mice compared with those of WT mice (Figure 3D).

AAV-VEGFC increases local lymphatic drainage and reduces alveolar bone loss in RA-associated periodontitis

To determine if overexpressed VEGFC promotes lymphatic vessel function in RA-associated periodontitis, 4-month-old TNF-Tg mice were administered a single injection of AAV-VEGFC virus or control AAV-GFP virus into the periodontal tissues of the maxillary first molar. All the TNF-Tg mice were euthanized 8 weeks post-injection, when they typically had severe periodontal inflammation and alveolar bone loss (Figure 1). The expression of AAV-VEGFC was confirmed by measuring human *VEGFC* in periodontal tissues of the maxillary first molar with human-specific primers. Human *VEGFC* was identified in periodontal tissues receiving AAV-VEGFC injection but not in periodontal tissues receiving AAV-GFP (Figure 4A). By IF, the area of $PDPN^+/\alpha SMA^-$ lymphatic capillaries decreased, whereas both the area and the number of $PDPN^+/\alpha SMA^+$ collecting LVs increased significantly in periodontal tissues of TNF-Tg mice receiving AAV-VEGFC compared with those of TNF-Tg mice receiving AAV-GFP (Figure 4B). Further, periodontal areas of TNF-Tg mice receiving AAV-VEGFC had markedly accelerated ICG clearance compared with those of TNF-Tg mice receiving AAV-GFP (Figure 4C). At time points 240, 330, and 420 min, the percentage of ICG clearance was significantly higher in periodontal tissues of TNF-Tg mice receiving AAV-VEGFC than in those of TNF-Tg mice receiving AAV-GFP, respectively (Figure 4C).

To determine if AAV-VEGFC had a beneficial effect on RA-associated periodontitis, μCT and morphometric analyses were performed on the mouse maxilla. Three-dimensional reconstruction images and volumetric measurements from μCT analysis revealed that the alveolar bone density was improved and the level of exposed root surface was attenuated in the maxillae of TNF-Tg mice receiving AAV-VEGFC compared with TNF-Tg mice receiving AAV-GFP (Figure 4D). Furthermore, morphometric measurements of

H&E-stained tissue sections showed that the distance from CEJ to ABC was significantly decreased in TNF-Tg mice receiving AAV-VEGFC compared with TNF-Tg mice receiving AAV-GFP (Figure 4E). TRAP-positive osteoclast surface was reduced, but ALP-positive osteoblast surface was increased in TNF-Tg mice receiving AAV-VEGFC compared with TNF-Tg mice receiving AAV-GFP (Figure 4F,G).

AAV-VEGFC increases local lymphatic drainage and reduces alveolar bone loss in ligature-induced periodontitis

To further demonstrate the relationship between lymphatic drainage and alveolar bone loss in periodontitis, we used the second mouse model, ligature-induced periodontitis [44]. Similar to RA-associated periodontitis, IF staining indicated that $PDPN^+/\alpha SMA^-$ lymphatic capillaries increased significantly, but $PDPN^+/\alpha SMA^+$ collecting LVs decreased dramatically in ligature-induced periodontitis compared with the control group (Figure 5A). Interestingly, both the area and the number of $PDPN^+/\alpha SMA^+$ collecting LVs were increased dramatically in ligature-induced periodontitis receiving AAV-VEGFC compared with that receiving AAV-GFP (Figure 5A). Further, periodontal areas of ligature-induced periodontitis had markedly delayed ICG clearance compared with the control group (Figure 5B). On the contrary, periodontal areas of ligature-induced periodontitis receiving AAV-VEGFC had significantly accelerated ICG clearance compared with those of ligature-induced periodontitis receiving AAV-GFP (Figure 5B).

Importantly, alveolar bone density by μCT analysis was decreased, whereas the distance from CEJ to ABC (in sections stained with H&E) and the TRAP-positive osteoclast surface were increased, in ligature-induced periodontitis compared with the control group (Figure 5C–E). In contrast, μCT analysis showed that alveolar bone density was increased, whereas the distance from CEJ to ABC in sections stained with H&E and the TRAP-positive osteoclast surface were decreased, in ligature-induced periodontitis receiving AAV-VEGFC compared with that receiving AAV-GFP (Figure 5C–E). Notably, the ALP-positive osteoblast surface was increased in ligature-induced periodontitis compared with the control group, which was even larger after AAV-VEGFC treatment, as indicated by ligature-induced periodontitis receiving AAV-VEGFC compared with that receiving AAV-GFP (Figure 5F).

Increased inflammatory cell infiltrations and decreased collecting lymphatic vessel formation in periodontal tissues from patients with chronic periodontitis

To determine the clinical relevance of our mouse findings, we examined the cell populations of gingival tissues from patients with chronic periodontitis or clinically healthy controls by flow cytometry. The data revealed that the percentages of $CD31^+$ endothelial cells (Figure 6A), $CD45^+CD14^+$ monocytes/macrophages (Figure 6B), and $CD19^+$ B cells (Figure 6C) were all higher in gingival tissues from patients with chronic periodontitis than in those from clinically healthy controls. In contrast, $CD3^+$ T-cell numbers in gingival tissues were not significantly different between patients with chronic periodontitis and healthy controls (Figure 6C).

To further examine the distribution and function of LVs in periodontal tissues, paraffin-embedded tissue sections either from patients with chronic periodontitis or from clinically

healthy controls were double-stained with anti-LYVE1 and anti-αSMA antibodies. Similar to the mouse findings, we observed three types of vessels: $LYVE1^{+}/\alpha SMA^{-}$ lymphatic capillaries, $LYVE1^{+}/\alpha SMA^{+}$ collecting LVs, and $LYVE1^{-}/\alpha SMA^{+}$ blood vessels in gingival tissues of healthy controls (Figure 6D,E). More $LYVE1^{+}/\alpha SMA^{-}$ lymphatic capillaries could be seen in gingival tissues of patients with chronic periodontitis than in those of clinically healthy controls (Figure 6E,F). In contrast, fewer $LYVE1^{+}/\alpha SMA^{+}$ collecting LVs were observed in patients with chronic periodontitis than in clinically healthy controls (Figure 6E,F).

Discussion

The lymphatic vasculature plays a crucial role in regulating the inflammatory response in various inflammatory diseases such as RA [35], periodontitis [16,20], skin inflammation [45], and inflammatory bowel disease [46,47]. However, most of these studies have not distinguished lymphatic capillaries from collecting LVs. This is important because lymphatic capillaries and collecting LVs have different morphology and functions. Here, we used murine periodontitis models including RA-associated periodontitis and ligature-induced periodontitis and demonstrated increased lymphatic capillaries and decreased collecting LVs in the periodontal tissues, accompanied by delayed lymph flow in periodontal tissues, increased TRAP-positive osteoclasts, and significant alveolar bone loss. The local administration of adeno-associated virus encoding VEGFC increased lymphatic collecting vessels, restored local lymph flow, and reduced alveolar bone loss in both models of periodontitis. Importantly, increased lymphatic capillaries and decreased collecting LVs were observed in gingival tissues of patients with chronic periodontitis compared with those of clinically healthy controls. Thus, our findings reveal the important role of local lymphatic drainage in periodontal inflammation-mediated alveolar bone loss.

At present, the molecular mechanisms underlying the involvement of the lymphatic vessel system in periodontitis have not been fully understood. VEGFC is the major growth factor that promotes lymphangiogenesis, and it exerts most of its effects through binding to its receptor, VEGFR3 [23,48]. VEGFD is the second VEGFR3 ligand that is structurally homologous to VEGFC [49]. A high VEGFC:VEGFD ratio correlates with the presence of lymphatic invasion in lung adenocarcinoma [50]. In the present study, we found increased gene expression levels of *Vegfc, Vegfd*, and the ratio of *Vegfc* to *Vegfd* mRNA levels, along with a decreased level of Vegfr3 in gingival tissues of TNF-Tg mice. Increased levels of VEGFR3 ligands in periodontitis are anticipated because various studies, including our own, reported high expression of VEGFC by inflammatory cells [51]. However, decreased *Vegfr3* expression is unexpected because it contradicts our understanding of inflammation-mediated lymphangiogenesis due to high VEGFC expression. This raises an important question: what is the impact of low *Vegfr3* levels in VEGFC-induced lymphangiogenesis? We suspect that the downregulation of *Vegfr3* may contribute to the inefficient action of *Vegfc* in the mouse model of periodontitis. For instance, massive amounts of VEGFC are needed to rescue the dominant negative effect of one mutated *Vegfr3* allele in Chy mice [52]. It is also possible that the experiment was stopped at a time when most of the lymphangiogenesis responses had already completed. Since little is known about the downregulation of *Vegfr3* in diseases, other complex mechanisms could also be involved and remain to be discovered.

Human VEGFC overexpression was used in the present study because it is fully functional in mouse tissues [35]. More importantly, the adenovirus-based gene therapy expressing human VEGFC directly in the damaged tissue is used for treatment of lymphedema in clinical trials (https://clinicaltrials.gov/ct2/results?term=lymfactin). Here, we expanded its application to the treatment of periodontitis. Our study demonstrates that AAV-VEGFC increases the area of $PDPN^{+}/\alpha SMA^{+}$ collecting LVs and promotes local lymphatic drainage. Since AAV-VEGFC could only produce a precursor protein of VEGFC instead of the functionally mature form, we assume that suitable proteases must have been endogenously available in the maxillary tissue to convert pro-VEGFC into one of the mature, active forms. Additionally, VEGFR3, the receptor for VEGFC, is also expressed in non-LECs such as neuronal progenitors, macrophages, and especially osteoblasts [53]. Thus, it is possible that the increased alveolar bone volume caused by AAV-VEGFC treatment may be partly due to the effects of VEGFC on osteoblast differentiation. Our study also indicated that the ALP-positive surface, as a percentage of the bone perimeter, was greater after AAV-VEGFC treatment. It would be beneficial to generate LEC-specific VEGFR3-overexpressing or knockout mice by crossing VEGFR3 transgenic mice or VEGFR3 floxed mice with Prox1-Cre mice and then perform ligature-induced periodontitis in the absence and presence of AAV-VEGFC administration. Such studies could define even better the role of VEGFC in lymphangiogenesis and its effect on periodontitis treatment.

Notably, although locally administered VEGFC reduced osteoclasts and alveolar bone loss and improved lymphatic drainage, the effects were incomplete, suggesting that either the concentration of VEGFC attained locally was insufficient or, more likely, other factors contribute to the inflammation, alveolar bone destruction, and lymphatic drainage. Another concern is that despite being the only FDA-approved probe for use in humans [54], indocyanine green (ICG) still has several limitations for NIR lymphatic imaging, due to aggregation and change of spectral properties of the dye after injection upon the monomerization caused by complexation with endogenous proteins [55]. This limitation has recently been addressed by precomplexing ICG with Kolliphor HS15 (Sigma-Aldrich), an FDA- and EMA-approved surfactant, which significantly increases ICG fluorescence intensity in the application for NIR lymphatic imaging [56]. We found a similar trend in mice injected with ICG–water compared with those injected with ICG–Kolliphor HS15. Importantly, at time point 420 min, the signal was very weak in WT mice injected with ICG–water, which remained relatively strong in WT mice injected with ICG–Kolliphor HS15 (supplementary material, Figure S1). We may use ICG plus Kolliphor HS15 instead of ICG alone for NIR lymphatic imaging to evaluate lymphatic function in a future study. Finally, we found that lymphatic capillaries are increased, whereas collecting LVs are not, in periodontal tissues of periodontitis. Much research has addressed the effect of inflammation on lymphatic vessels without distinguishing lymphatic capillaries and collecting LVs. Our data implied that effects on lymphatic capillaries and collecting LVs do not always go hand-in-hand, although such in-sync responses have been reported in patients with severe osteoarthritis [7]. Furthermore, instead of increasing vessel density, collecting LVs usually change their contractile behavior in response to inflammatory conditions [57]. In the future, we may pay attention to the contractile behavior of collecting LVs in our research.

In summary, using murine models of periodontitis and patient tissues, we have demonstrated that lymphatic dysfunction within the periodontal microenvironment contributes to alveolar bone loss in periodontitis. Local VEGFC overexpression increases the area of collecting LVs, promotes local lymphatic drainage, and reduces alveolar bone loss in both models of periodontitis. Thus, our findings reveal an important role of local lymphatic drainage in periodontal inflammation-mediated alveolar bone loss.

Supplementary Material

Refer to Web version on PubMed Central for supplementary material.

Acknowledgements

This research was supported by grants from the National Natural Science Foundation of China (81670965 to WS and 81970961 to HW), the Natural Science Foundation of Jiangsu Province in China (BK20180034 to WS and BK20191346 to HW), and the National Key Research and Development Program of China (2018YFA0800804). LX is supported by a grant from National Institutes of Health PHS awards, USA (R01AG059775). The project was also supported by Jiangsu Innovation and Entrepreneurship Training Program for College Students (201910312003Z to HZ).

References

1. Trevaskis NL, Kaminskas LM, Porter CJ. From sewer to saviour – targeting the lymphatic system to promote drug exposure and activity. Nat Rev Drug Discov 2015; 14: 781–803. [PubMed: 26471369]
2. Bouta EM, Bell RD, Rahimi H, et al. Targeting lymphatic function as a novel therapeutic intervention for rheumatoid arthritis. Nat Rev Rheumatol 2018; 14: 94–106. [PubMed: 29323343]
3. Gucciardo E, Loukovaara S, Korhonen A, et al. The microenvironment of proliferative diabetic retinopathy supports lymphatic neovascularization. J Pathol 2018; 245: 172–185. [PubMed: 29536540]
4. Alitalo K The lymphatic vasculature in disease. Nat Med 2011; 17: 1371–1380. [PubMed: 22064427]
5. Voisin MB, Nourshargh S. Neutrophil trafficking to lymphoid tissues: physiological and pathological implications. J Pathol 2019; 247: 662–671. [PubMed: 30584795]
6. Gerner MY, Torabi-Parizi P, Germain RN. Strategically localized dendritic cells promote rapid T cell responses to lymph-borne particulate antigens. Immunity 2015; 42: 172–185. [PubMed: 25607462]
7. Shi J, Liang Q, Zuscik M, et al. Distribution and alteration of lymphatic vessels in knee joints of normal and osteoarthritic mice. Arthritis Rheumatol 2014; 66: 657–666. [PubMed: 24574226]
8. Liao S, Padera TP. Lymphatic function and immune regulation in health and disease. Lymphat Res Biol 2013; 11: 136–143. [PubMed: 24024577]
9. Saccucci M, Di Carlo G, Bossu M, et al. Autoimmune diseases and their manifestations on oral cavity: diagnosis and clinical management. J Immunol Res 2018; 2018: 6061825. [PubMed: 29977929]
10. Bingham CO 3rd,Moni M. Periodontal disease and rheumatoid arthritis: the evidence accumulates for complex pathobiologic interactions. Curr Opin Rheumatol 2013; 25: 345–353. [PubMed: 23455329]
11. Araújo VM, Melo IM, Lima V. Relationship between periodontitis and rheumatoid arthritis: review of the literature. Mediators Inflamm 2015; 2015: 259074. [PubMed: 26347200]
12. Smolen JS, Aletaha D, Barton A, et al. Rheumatoid arthritis. Nat Rev Dis Primers 2018; 4: 18001. [PubMed: 29417936]
13. Soler Palacios B, Estrada-Capetillo L, Izquierdo E, et al. Macrophages from the synovium of active rheumatoid arthritis exhibit an activin A-dependent pro-inflammatory profile. J Pathol 2015; 235: 515–526. [PubMed: 25319955]

14. Kim D, Lee G, Huh YH, et al. NAMPT is an essential regulator of RA-mediated periodontal inflammation. J Dent Res 2017; 96: 703–711. [PubMed: 28165872]
15. Abe T, Hajishengallis G. Optimization of the ligature-induced periodontitis model in mice. J Immunol Methods 2013; 394: 49–54. [PubMed: 23672778]
16. Mkonyi LE, Bletsa A, Bolstad AI, et al. Gingival lymphatic drainage protects against *Porphyromonas gingivalis*-induced bone loss in mice. Am J Pathol 2012; 181: 907–916. [PubMed: 22901755]
17. Matsumoto Y, Zhang B, Kato S. Lymphatic networks in the periodontal tissue and dental pulp as revealed by histochemical study. Microsc Res Tech 2002; 56: 50–59. [PubMed: 11810706]
18. Fujimura A, Nozaka Y. Analysis of the three-dimensional lymphatic architecture of the periodontal tissue using a new 3D reconstruction method. Microsc Res Tech 2002; 56: 60–65. [PubMed: 11810707]
19. Zhang B, Miura M, Ji RC, et al. Structural organization and fine distribution of lymphatic vessels in periodontal tissues of the rat and monkey: a histochemical study. Okajimas Folia Anat Jpn 2000; 77: 93–107. [PubMed: 11111377]
20. Papadakou P, Bletsa A, Yassin MA, et al. Role of hyperplasia of gingival lymphatics in periodontal inflammation. J Dent Res 2017; 96: 467–476. [PubMed: 28081372]
21. Mkonyi LE, Bakken V, Sovik JB, et al. Lymphangiogenesis is induced during development of periodontal disease. J Dent Res 2012; 91: 71–77. [PubMed: 21979132]
22. Blasco-Baque V, Garidou L, Pomie C, et al. Periodontitis induced by *Porphyromonas gingivalis* drives periodontal microbiota dysbiosis and insulin resistance via an impaired adaptive immune response. Gut 2017; 66: 872–885. [PubMed: 26838600]
23. Achen MG, Mann GB, Stacker SA. Targeting lymphangiogenesis to prevent tumour metastasis. Br J Cancer 2006; 94: 1355–1360. [PubMed: 16641900]
24. Jiang CK, Epstein HS, Tomic M, et al. Functional comparison of the upstream regulatory DNA sequences of four human epidermal keratin genes. J Invest Dermatol 1991; 96: 162–167. [PubMed: 1704037]
25. Ushijima N, Inoue K, Domon T, et al. Distribution and organization of lymphatic vessels in the mouse gingiva: an immunohistochemical study with LYVE-1. Arch Oral Biol 2008; 53: 652–658. [PubMed: 18316062]
26. Sun W, Zhang H, Wang H, et al. Targeting Notch-activated M1 macrophages attenuates joint tissue damage in a mouse model of inflammatory arthritis. J Bone Miner Res 2017; 32: 1469–1480. [PubMed: 28256007]
27. Keffer J, Probert L, Cazlaris H, et al. Transgenic mice expressing human tumour necrosis factor: a predictive genetic model of arthritis. EMBO J 1991; 10: 4025–4031. [PubMed: 1721867]
28. Sun W, Meednu N, Rosenberg A, et al. B cells inhibit bone formation in rheumatoid arthritis by suppressing osteoblast differentiation. Nat Commun 2018; 9: 5127. [PubMed: 30510188]
29. Bell R, Wood R, Chakkalakal J, et al. Increased morbidity and mortality in female versus male tumor necrosis factor-transgenic mice [abstract]. Arthritis Rheumatol 2015; 67(suppl 10). https://acrabstracts.org/abstract/increased-morbidity-and-mortality-in-female-versus-male-tumor-necrosis-factor-transgenic-mice/ [accessed 27 May 2020].
30. Kataoka K, Ekuni D, Tomofuji T, et al. Visualization of oxidative stress induced by experimental periodontitis in Keap1-dependent oxidative stress detector-luciferase mice. Int J Mol Sci 2016; 17: 1907. [PubMed: 27854327]
31. Mahanonda R, Champaiboon C, Subbalekha K, et al. Human memory B cells in healthy gingiva, gingivitis, and periodontitis. J Immunol 2016; 197: 715–725. [PubMed: 27335500]
32. Wang H, Hu Z, Wu J, et al. Sirt1 promotes osteogenic differentiation and increases alveolar bone mass via Bmi1 activation in mice. J Bone Miner Res 2019; 34: 1169–1181. [PubMed: 30690778]
33. Wang H, LvC, Gu Y, et al. Overexpressed Sirt1 in MSCs promotes dentin formation in Bmi1-deficient mice. J Dent Res 2018; 97: 1365–1373. [PubMed: 29932801]
34. Wang W, Lin X, Xu H, et al. Attenuated joint tissue damage associated with improved synovial lymphatic function following treatment with bortezomib in a mouse model of experimental posttraumatic osteoarthritis. Arthritis Rheumatol 2019; 71: 244–257. [PubMed: 30144298]

35. Zhou Q, Guo R, Wood R, et al. Vascular endothelial growth factor C attenuates joint damage in chronic inflammatory arthritis by accelerating local lymphatic drainage in mice. Arthritis Rheum 2011; 63: 2318–2328. [PubMed: 21538325]
36. Gao B, Chen W, Hao L, et al. Inhibiting periapical lesions through AAV-RNAi silencing of cathepsin K. J Dent Res 2013; 92: 180–186. [PubMed: 23166044]
37. Tammela T, Saaristo A, Holopainen T, et al. Therapeutic differentiation and maturation of lymphatic vessels after lymph node dissection and transplantation. Nat Med 2007; 13: 1458–1466. [PubMed: 18059280]
38. Morisada T, Oike Y, Yamada Y, et al. Angiopoietin-1 promotes LYVE-1-positive lymphatic vessel formation. Blood 2005; 105: 4649–4656. [PubMed: 15705793]
39. Saharinen P, Tammela T, Karkkainen MJ, et al. Lymphatic vasculature: development, molecular regulation and role in tumor metastasis and inflammation. Trends Immunol 2004; 25: 387–395. [PubMed: 15207507]
40. Noda Y, Amano I, Hata M, et al. Immunohistochemical examination on the distribution of cells expressed lymphatic endothelial marker podoplanin and LYVE-1 in the mouse tongue tissue. Acta Histochem Cytochem 2010; 43: 61–68. [PubMed: 20514293]
41. Li J, Kuzin I, Moshkani S, et al. Expanded $CD23^{+}/CD21^{hi}$ B cells in inflamed lymph nodes are associated with the onset of inflammatory-erosive arthritis in TNF-transgenic mice and are targets of anti-CD20 therapy. J Immunol 2010; 184: 6142–6150. [PubMed: 20435928]
42. Guo R, Zhou Q, Proulx ST, et al. Inhibition of lymphangiogenesis and lymphatic drainage via vascular endothelial growth factor receptor 3 blockade increases the severity of inflammation in a mouse model of chronic inflammatory arthritis. Arthritis Rheum 2009; 60: 2666–2676. [PubMed: 19714652]
43. Huggenberger R, Ullmann S, Proulx ST, et al. Stimulation of lymphangiogenesis via VEGFR-3 inhibits chronic skin inflammation. J Exp Med 2010; 207: 2255–2269. [PubMed: 20837699]
44. Tsukasaki M, Komatsu N, Nagashima K, et al. Host defense against oralmicrobiotaby bone-damaging T cells. Nat Commun 2018; 9: 701. [PubMed: 29453398]
45. Huggenberger R, Siddiqui SS, Brander D, et al. An important role of lymphatic vessel activation in limiting acute inflammation. Blood 2011; 117: 4667–4678. [PubMed: 21364190]
46. Schwager S, Detmar M. Inflammation and lymphatic function. Front Immunol 2019; 10: 308. [PubMed: 30863410]
47. Pedica F, Ligorio C, Tonelli P, et al. Lymphangiogenesis in Crohn's disease: an immunohistochemical study using monoclonal antibody D2–40. Virchows Arch 2008; 452: 57–63. [PubMed: 18040712]
48. Qin TT, Xu GC, Qi JW, et al. Tumour necrosis factor superfamily member 15 (Tnfsf15) facilitates lymphangiogenesis via up-regulation of Vegfr3 gene expression in lymphatic endothelial cells. J Pathol 2015; 237: 307–318. [PubMed: 26096340]
49. Achen MG, Jeltsch M, Kukk E, et al. Vascular endothelial growth factor D (VEGF-D) is a ligand for the tyrosine kinases VEGF receptor 2 (Flk1) and VEGF receptor 3 (Flt4). Proc Natl Acad Sci U S A 1998; 95: 548–553. [PubMed: 9435229]
50. Niki T, Iba S, Tokunou M, et al. Expression of vascular endothelial growth factors A, B, C, and D and their relationships to lymph node status in lung adenocarcinoma. Clin Cancer Res 2000; 6: 2431–2439. [PubMed: 10873096]
51. Zhang Q, Lu Y, Proulx ST, et al. Increased lymphangiogenesis in joints of mice with inflammatory arthritis. Arthritis Res Ther 2007; 9: R118. [PubMed: 17997858]
52. Karkkainen MJ, Saaristo A, Jussila L, et al. A model for gene therapy of human hereditary lymphedema. Proc Natl Acad Sci U S A 2001; 98: 12677–12682. [PubMed: 11592985]
53. Watanabe C, Matsushita J, Azami T, et al. Generating Vegfr3 reporter transgenic mouse expressing membrane-tagged Venus for visualization of VEGFR3 expression in vascular and lymphatic endothelial cells. PLoS One 2019; 14: e0210060. [PubMed: 30601868]
54. Weiler M, Dixon JB. Differential transport function of lymphatic vessels in the rat tail model and the long-term effects of Indocyanine Green as assessed with near-infrared imaging. Front Physiol 2013; 4: 215. [PubMed: 23966950]

55. Bunschoten A, Buckle T, Kuil J, et al. Targeted non-covalent self-assembled nanoparticles based on human serum albumin. Biomaterials 2012; 33: 867–875. [PubMed: 22024362]

56. Polomska AK, Proulx ST, Brambilla D, et al. Minimally invasive method for the point-of-care quantification of lymphatic vessel function. JCI Insight 2019; 4: e126515. [PubMed: 30667371]

57. Liao S, von der Weid PY. Inflammation-induced lymphangiogenesis and lymphatic dysfunction. Angiogenesis 2014; 17: 325–334. [PubMed: 24449090]

58. Sun W, Wu J, Huang L, et al. PTHrP nuclear localization and carboxyl terminus sequences modulate dental and mandibular development in part via the action of p27. Endocrinology 2016; 157: 1372–1384. [PubMed: 26859332]

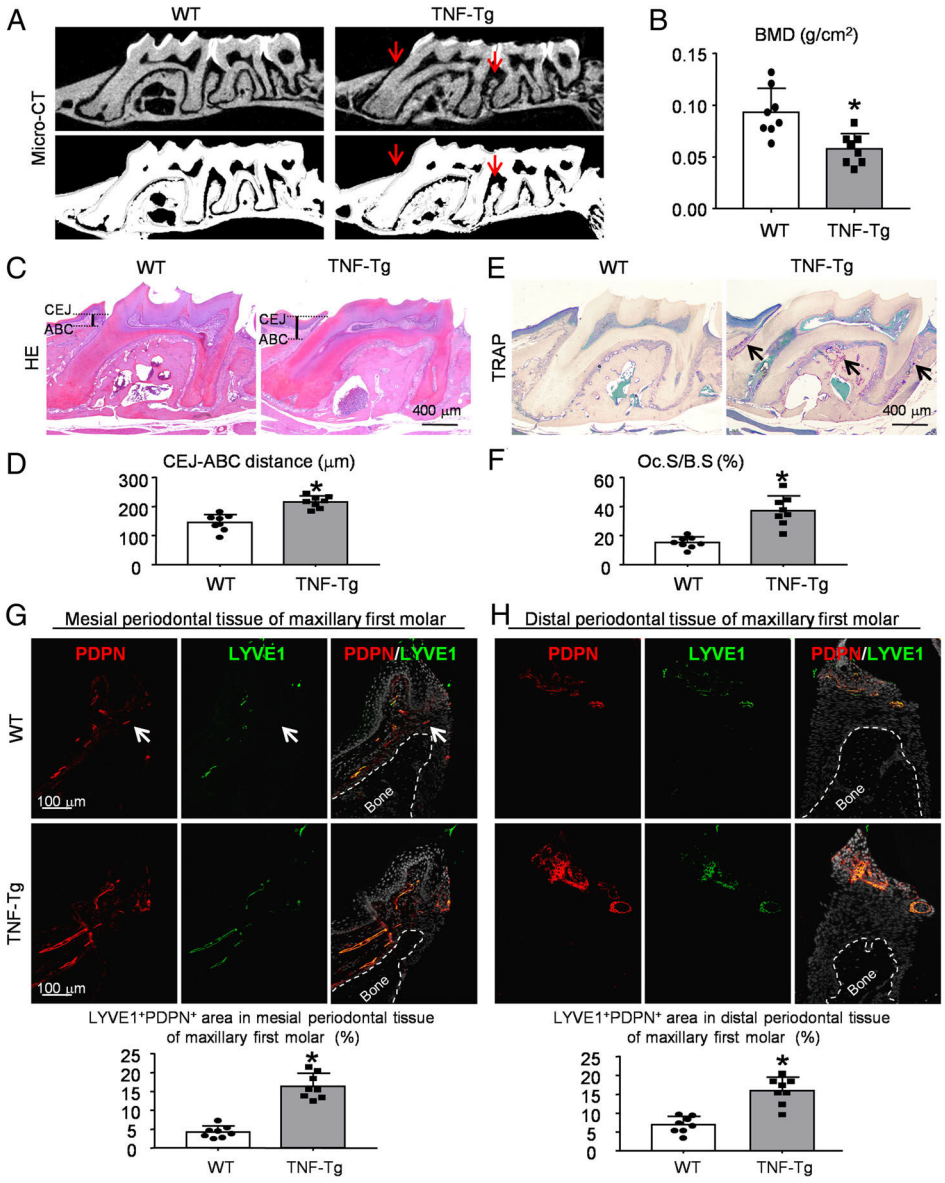

Figure 1.

Increased alveolar bone loss, TRAP-positive osteoclast activity, and lymphatic areas in RA-associated periodontitis. Six-month-old TNF-Tg RA mice and their WT littermates were used. (A) Representative 3D scanned sections (upper panels) and reconstructed sections (lower panels) along the longitudinal direction of the maxillae. Red arrows indicate the alveolar bone crest. (B) Bone mineral density (BMD, g/cm^2) of A was analyzed. (C) Representative images of H&E-stained paraffin sections. (D) Measurement of the bone levels by comparing the distance from the cemento-enamel junction (CEJ) to the alveolar bone crest (ABC) in μm was determined. (E) Representative images of TRAP-stained paraffin sections. (F) Oc.S/B.S (%): the percentage of alveolar bone surface covered by TRAP-positive osteoclasts (indicated by black arrows) was determined by morphological analysis. (G, H) Paraffin sections of maxillae were subjected to IF for LYVE1 (green) and PDPN (red) for lymphatics. White dashed lines indicate the bone surface and white arrows

the $LYVE1^{-}/PDPN^{+}$ vessels. Quantification of the $LYVE1^{+}PDPN^{+}$ area/tissue area (%) in mesial (G) or distal (H) periodontal tissue of the maxillary first molar was determined. $*p < 0.05$ versus WT. Eight mice and their WT controls were included in each experiment. A two-tailed unpaired Student's *t*-test was performed.

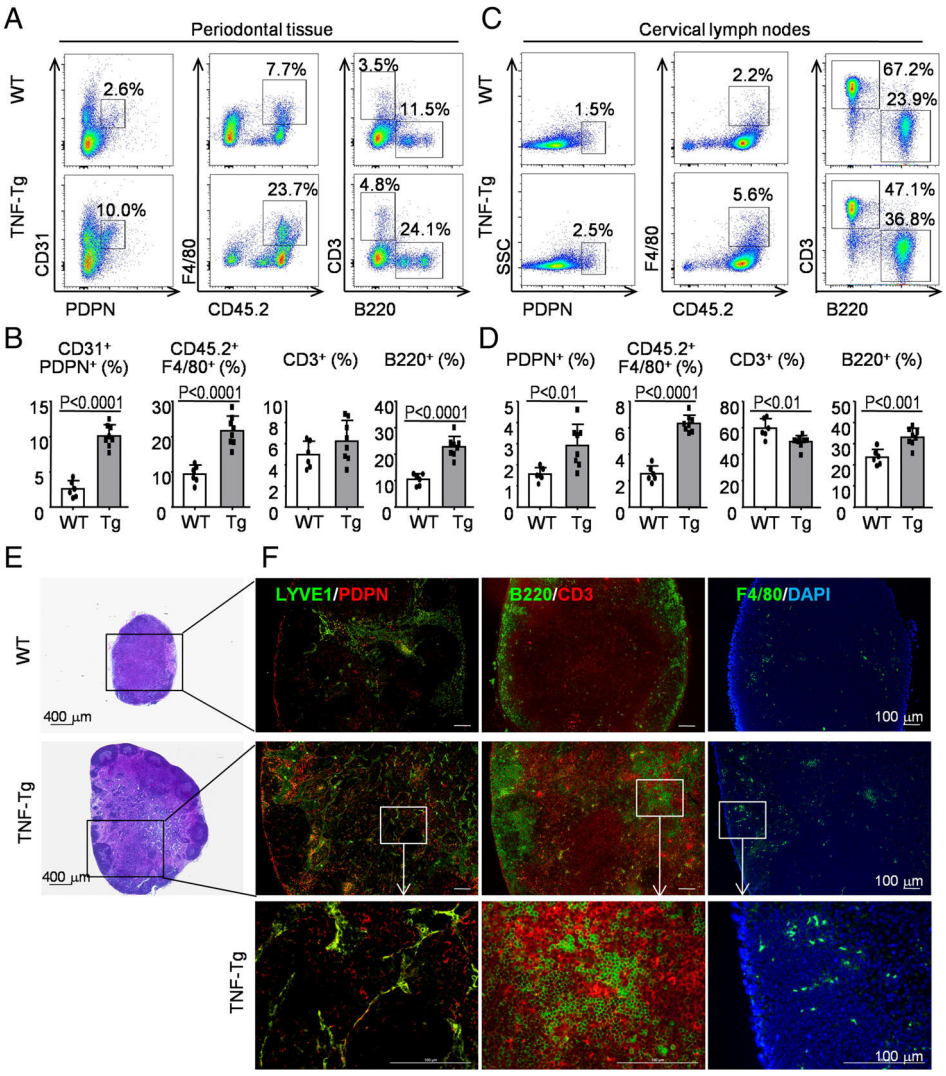

Figure 2.

Numbers of lymphatic endothelial cells, macrophages, and B cells are increased in periodontal tissues and in the cervical (draining) lymph nodes in RA-associated periodontitis. Six-month-old TNF-Tg RA mice and their WT littermates were used. (A) Cells from periodontal tissue were collected and analyzed by flow cytometry. Representative dot-plot shows the population of various cell subsets. (B) Subpopulations of cells in the periodontal tissue. (C) Cells from cervical lymph nodes were collected and analyzed by flow cytometry. Representative dot-plot shows the population of various cell subsets. (D) Subpopulations of cells in the cervical lymph nodes. Paraffin sections of cervical lymph nodes were H&E-stained (E) and adjacent sections were subjected to IF (F) for LYVE1 (green) and PDPN (red) for LVs (left-hand panel), for B220 (green) for B cells and CD3 (red) Ab for T cells (middle panel), with F4/80 (green) for macrophages (right-hand panel). Between six and eight mice per group were included in each experiment. Two-tailed unpaired Student's *t*-tests were performed.

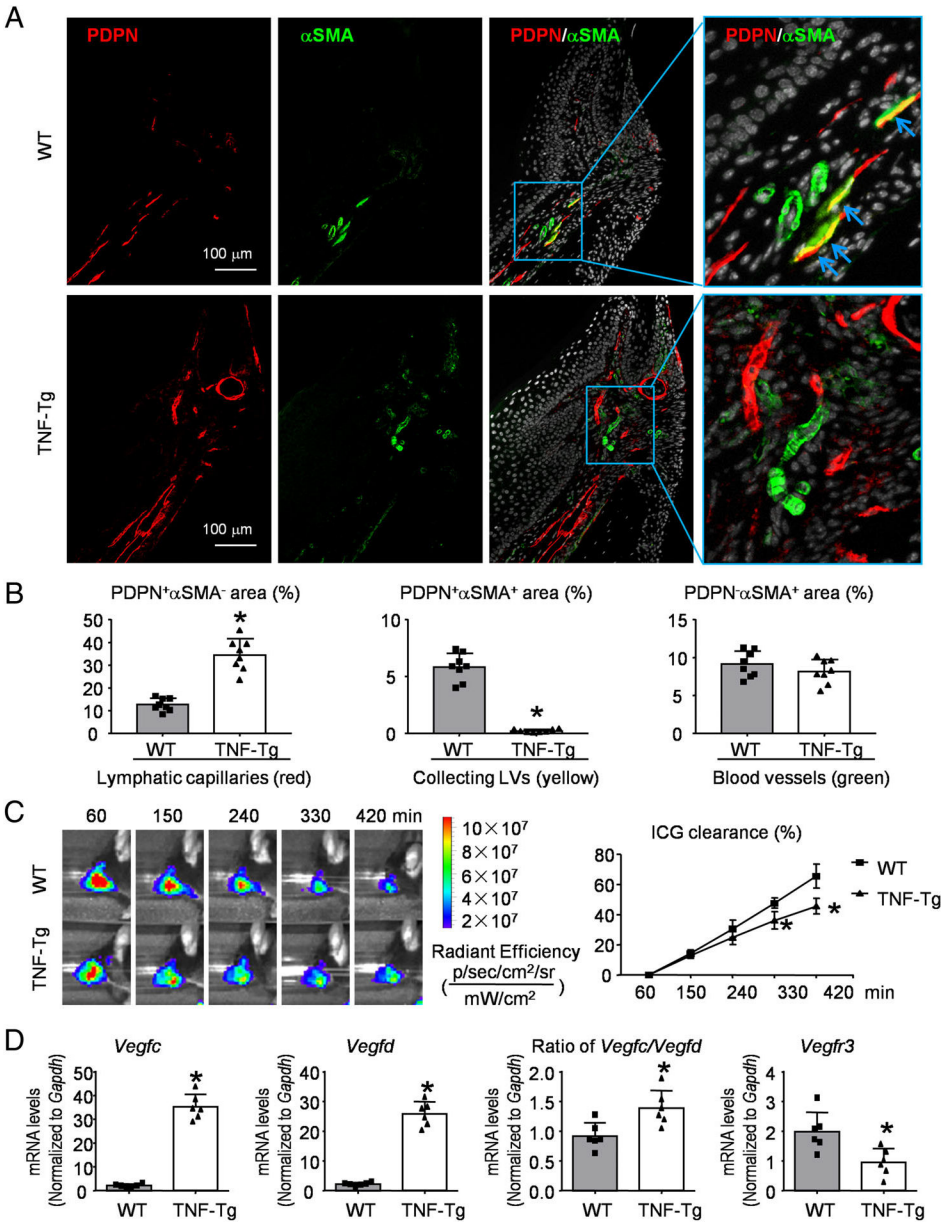

Figure 3.

Decreased collecting lymphatic vessels and lymph flow in periodontal tissues of RA-associated periodontitis. Six-month-old TNF-Tg RA mice and their WT littermates were used. (A) Paraffin sections of maxillae were subjected to IF for PDPN (red) and αSMA (green). Representative images of periodontal tissue showing the distribution of $PDPN^{+}/\alpha SMA^{-}$ lymphatic capillaries (red), $PDPN^{+}/\alpha SMA^{+}$ collecting LVs (yellow, indicated by blue arrows), and $PDPN^{-}/\alpha SMA^{+}$ blood vessels (green). (B) Quantification of the $PDPN^{+}\alpha SMA^{-}$ area, $PDPN^{+}\alpha SMA^{+}$ area or $PDPN^{-}\alpha SMA^{+}$ area to tissue area (%) was determined. (C) An example of *in vivo* washout of ICG: 1 μl (0.5 μg/μl) of ICG was injected sub-epithelially in the buccal oral mucosa to the maxillary first molar area. The total fluorescence in the entire posterior facial area was measured using an optical imager (IVIS Spectrum) at 60 min post-injection. The measurement was repeated every 90 min

for a 7-h period. ICG clearance (%) was quantified. Values shown are mean ± SEM. (D) Gene expression levels were measured by RT-qPCR. Values were calculated as CT (gene of interest)/2 – CT (*Gapdh*) × 100. *$p < 0.05$ versus WT at the same time point. Between six and eight mice per group were included in each experiment. Two-tailed unpaired Student's *t*-tests were performed.

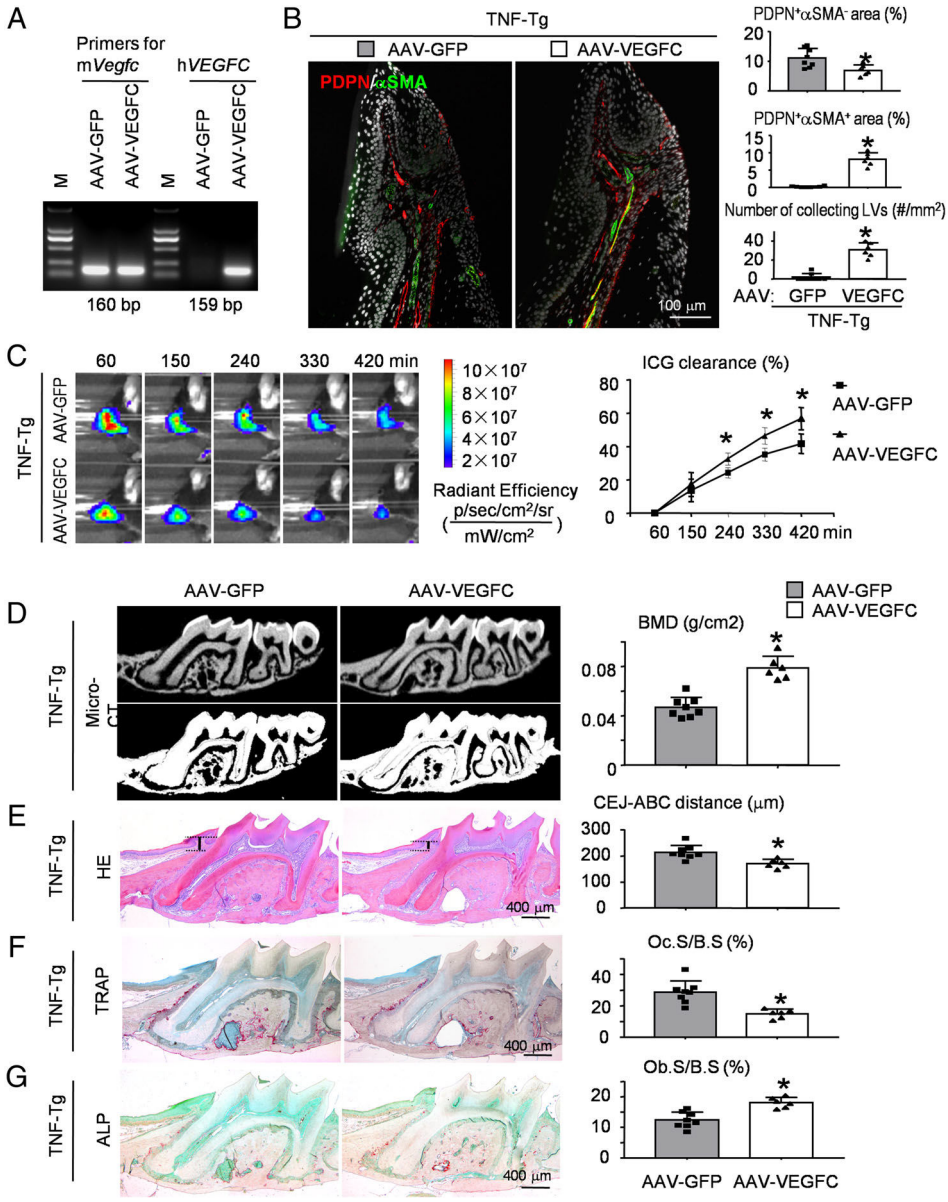

Figure 4.

AAV-VEGFC increases local lymphatic drainage and reduces alveolar bone loss in RA-associated periodontitis. Four-month-old TNF-Tg mice received local injection of AAV-GFP control virus (left maxillary) or AAV-VEGFC virus (right maxillary) into periodontal tissues of the left and right maxillary first molar, respectively. Two months after viral injection, mice were sacrificed and analyzed. (A) Expression of virus-encoded human VEGFC in periodontal tissues of TNF-Tg mice. (B) Paraffin sections of maxillae were subjected to IF for PDPN (red) and αSMA (green). Representative images of periodontal tissue showing the distribution of $PDPN^+/\alpha SMA^-$ lymphatic capillaries (red), $PDPN^+/\alpha SMA^+$ collecting LVs (yellow), and $PDPN^-/\alpha SMA^+$ blood vessels (green). Quantification of the $PDPN^+\alpha SMA^-$ area or $PDPN^+\alpha SMA^+$ area to tissue area (%) was determined. The number of $PDPN^+\alpha SMA^+$ collecting LVs per mm^2 tissue areas ($\#/mm^2$) was calculated.

(C) An example of in vivo washout of ICG in periodontal tissues reflecting lymph flow through all time points. ICG clearance (%) was quantified. Values shown are mean ± SEM. *$p < 0.05$ versus AAV-GFP control virus at the same time point. (D) Representative 3D scanned sections (upper panels) and reconstructed sections (lower panels) along the longitudinal direction of the maxillae. Bone mineral density (BMD, g/cm^2) was analyzed. (E) Representative images of H&E-stained paraffin sections. Measurement of the bone levels by comparing the distance from the cemento-enamel junction (CEJ) to the alveolar bone crest (ABC) in μm was determined. (F) Representative images of TRAP-stained paraffin sections. The percentage of alveolar bone surface covered by osteoclasts (Oc.S/B.S) was determined. (G) Representative images of ALP-stained paraffin sections. The percentage of alveolar bone surface covered by osteoblasts (Ob.S/B.S) was determined. *$p < 0.05$ versus AAV-GFP control virus. N = 6–8. A two-tailed unpaired Student's *t*-test was performed.

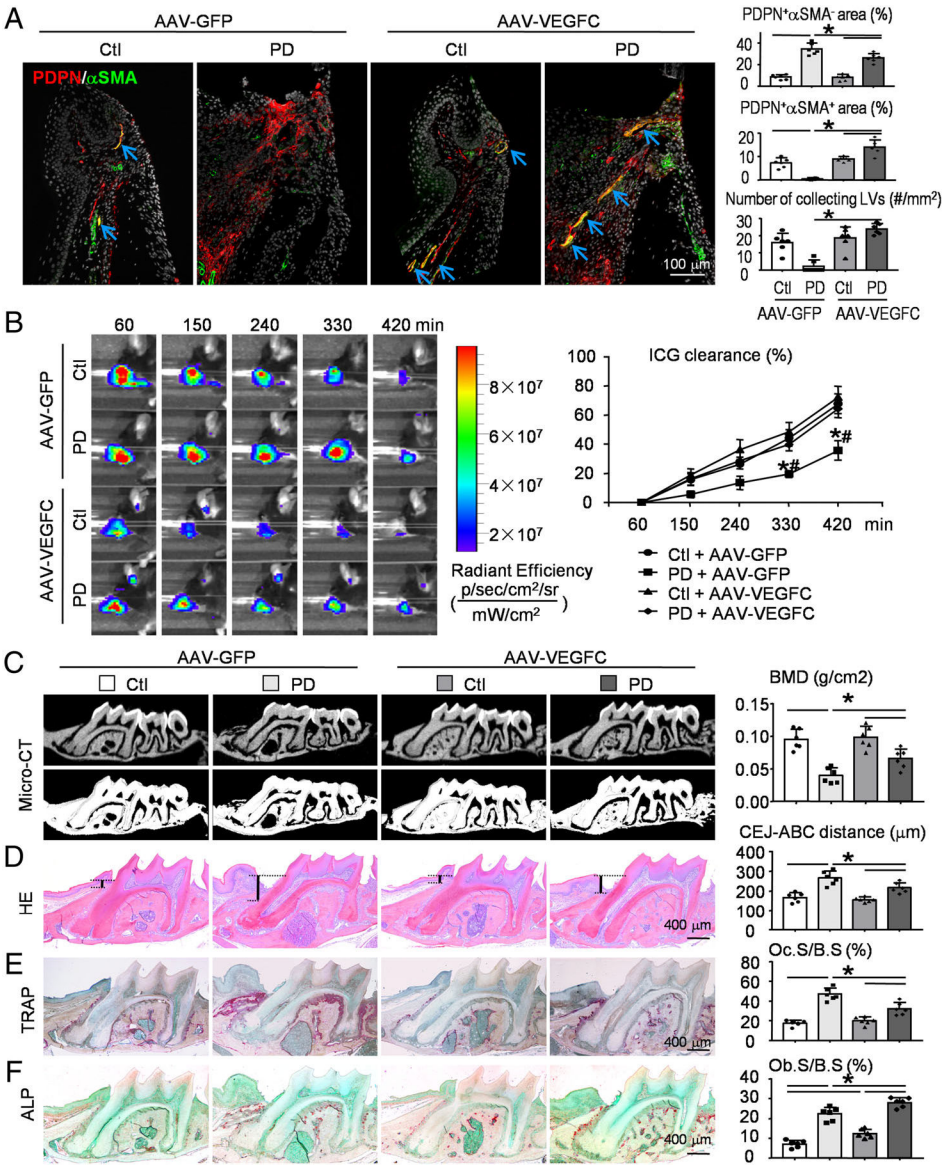

Figure 5.

AAV-VEGFC increases local lymphatic drainage and reduces alveolar bone loss in ligature-induced periodontitis. Two-month-old WT mice were randomly divided into two groups (six mice per group). One group received local injection of AAV-GFP control virus in periodontal tissues of both the left and right maxillary first molar. Another group received AAV-VEGFC virus injection. Two weeks later, a 5–0 silk ligature was tied around the right maxillary first molar and the contralateral tooth was left unligated to serve as the baseline control. All the mice were sacrificed and analyzed 2 weeks after placement of the ligature. (A) Paraffin sections of maxillae were subjected to IF for PDPN (red) and αSMA (green). Representative images of periodontal tissue showing the distribution of $PDPN^{+}/\alpha SMA^{-}$ lymphatic capillaries (red), $PDPN^{+}/\alpha SMA^{+}$ collecting LVs (yellow), and $PDPN^{-}/\alpha SMA^{+}$ blood vessels (green). Quantification of the $PDPN^{+}\alpha SMA^{-}$ area or $PDPN^{+}\alpha SMA^{+}$ area to tissue area (%) was determined. The number of $PDPN^{+}\alpha SMA^{+}$ collecting LVs per

mm^2 tissue areas (#/mm^2) was calculated. (B) An example of in vivo washout of ICG in periodontal tissues reflecting lymph flow through all time points. ICG clearance (%) was quantified. Values shown are mean ± SEM. *$p < 0.05$ versus control + AAV-GFP, $^{\#}p < 0.05$ versus periodontitis + AAV-VEGFC, at the same time point. (C) Representative 3D scanned sections (upper panels) and reconstructed sections (lower panels) along the longitudinal direction of the maxillae. Bone mineral density (BMD, g/cm^2) was analyzed. (D) Representative images of H&E-stained paraffin sections. Measurement of the bone levels by comparing the distance from the cemento-enamel junction (CEJ) to the alveolar bone crest (ABC) in μm was determined. (E) Representative images of TRAP-stained paraffin sections. The percentage of alveolar bone surface covered by osteoclasts (Oc.S/B.S) was determined. (F) Representative images of ALP-stained paraffin sections. The percentage of alveolar bone surface covered by osteoblasts (Ob.S/B.S) was determined. *$p < 0.05$ in the indicated groups. $N = 6$. One-way ANOVA followed by Dunnett's *post hoc* multiple comparisons test was performed.

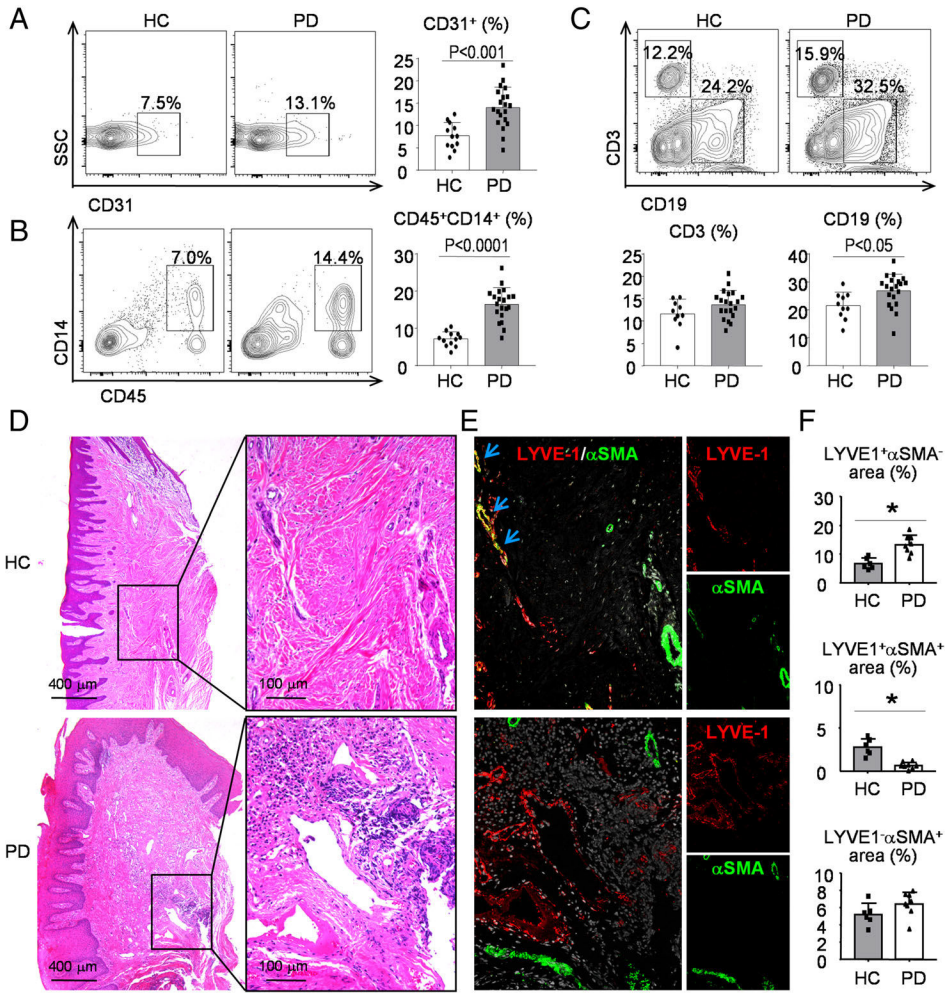

Figure 6.

Increased inflammatory cell infiltrations and decreased collecting lymphatic vessel formation in periodontal tissues from patients with chronic periodontitis. Gingival tissue specimens from patients with chronic periodontitis or clinically healthy controls were used. (A–C) Cells from tissue specimens were collected and analyzed by flow cytometry. Representative dot-plot shows (A) the population of $CD31^+$ endothelial cells, (B) $CD45^+CD14^+$ monocytes/macrophages, and (C) $CD3^+$ T cells and $CD19^+$ B cells. N = 12–20. A two-tailed unpaired Student's t-test was performed. (D) Paraffin sections were H&E-stained and adjacent sections were subjected to IF with (E) anti-LYVE1 (red) and anti-αSMA (green) Abs. Representative images showing the distribution of $LYVE1^+/\alpha SMA^-$ lymphatic capillaries (red), $LYVE1^+/\alpha SMA^+$ collecting LVs (yellow, indicated by blue arrows), and $LYVE1^-/\alpha SMA^+$ blood vessels (green). (F) Quantification of the $LYVE1^+\alpha SMA^-$ area, $LYVE1^+\alpha SMA^+$ area or $LYVE1^-\alpha SMA^+$ area to tissue area (%) was determined. Patients with chronic periodontitis (n = 8) and their controls (n = 6) were included in this experiment. The experiment was repeated at least once, with representative images shown. A two-tailed unpaired Student's t-test was performed.